Microstructure of Stainless Steel Single-Crystal Electron Beam Welds

S.A. DAVID, J.M. VITEK, M. RAPPAZ, and L.A. BOATNER

Previously developed techniques by the authors for the microstructural analysis of welds, that included the effects of both the growth crystallography and the weld pool shape, are applied to several cases involving the single-crystal electron beam welding of an Fe-15Ni-15Cr alloy. This evaluation of weld microstructures and associated dendritic growth patterns is based on a three-dimensional (3-D) geometrical analysis. The present study includes examination of the effects observed in overlapping, multipass autogenous welds and butt welds of two single crystals with different orientations, as well as effects due to variations in the welding speed. Weld pool shapes were found to change significantly with increasing welding speed—becoming narrower in cross section but more elongated in the welding direction. Additionally, all electron beam welds showed evidence of a plateau region in the center of the weld pool. The pool shapes, however, were found to be independent of the crystallographic orientation. Therefore, it is possible to extend the pool shape results to crystals welded in any orientation and even to polycrystals. The overlapping multipass welds showed remarkable reproducibility from pass to pass and duplicated the structural patterns found in single-pass welds. The similarity in dendritic patterns within each pass indicated that the weld pool shapes were identical in all of the passes. The microstructure of butt welds of two single crystals with different relative orientations showed a remarkable relationship to that associated with each individual crystallographic orientation, and the microstructure was, in effect, simply a composite of two single-pass microstructures. Additional microstructural details were also examined. The tendency toward branching of dendrites was associated with the transition from one dendrite growth orientation to another. It was also found that the nonpenetrating welds exhibited a small protrusion at the bottom of the weld. It is suggested that the modeling of weld pool shapes can be directly evaluated by comparing the predicted dendritic growth patterns based on the modeled shapes with the actual experimentally observed dendritic growth patterns.

I. INTRODUCTION

THE development of the fusion-zone grain structure in a weld is primarily controlled by the base-metal grain structure and the welding conditions. In welds, the base metal acts as a substrate upon which growth of the solid phase occurs; *i.e.*, the initial solidification occurs epitaxially at partially melted grains in the base metal.[1–4] Both crystallographic effects and welding conditions (*e.g.*, welding speed and other process parameters, and heat and fluid flow) can influence the development of microstructures in the fusion zone. Specifically, crystallographic effects will influence grain growth by favoring growth along particular crystallographic directions, namely, "the easy growth directions."[1,3,5–7] For cubic metals such as the austenitic stainless steel considered in this paper, the easy growth directions are the ⟨100⟩ directions. Conditions for growth are optimum when one of the easy growth directions coincides with the heat flow direction, in which case the undercooling of the associated dendrite tips is a minimum. Accordingly, among the randomly oriented grains in a polycrystalline specimen, those grains that have one of their ⟨100⟩ crystallographic axes most closely aligned with the heat flow direction will be favored. Welding conditions and heat flow significantly influence the final grain structure in that they determine the weld pool shape. The solid/liquid interface is essentially perpendicular to the heat flow direction, and therefore, the weld pool shape determines the optimum growth direction. In addition, convection within the molten pool varies with welding conditions and may also influence the grain development.*

*In this paper, we will not consider the effects of convection fluid flow in any detail.

It is relatively difficult to understand fully the development of fusion-zone microstructures in welds of polycrystalline specimens, because details of the grain growth selection process and the three-dimensional (3-D) pool shape are obscured by the multitude of grains and crystal orientations that are present in polycrystalline materials. The complexity of a polycrystalline fusion-zone microstructure in an austenitic stainless steel weld metal is illustrated in Figure 1. For polycrystalline materials, a large range of crystal orientations is present, and different crystals may actively grow at different stages of the weld pool solidification. In the absence of a fixed crystal orientation reference system everywhere along the weld pool solidification front, the only information on the weld pool

S.A. DAVID, Group Leader, Materials Joining Group, Metals and Ceramics Division, J.M. VITEK, Research Staff Member, Microscopy and Microanalytical Sciences Group, Metals and Ceramics Division, and L.A. BOATNER, Section Head, Ceramics and Interfaces Section, Solid State Division, are with Oak Ridge National Laboratory, Oak Ridge, TN 37831. M. RAPPAZ, formerly Visiting Scientist, Solid State Division, Oak Ridge National Laboratory, is Group Leader, Modeling of Solidification Processes Group, with the Laboratoire de Métallurgie Physique, Ecole Polytechnique Fédérale de Lausanne, Lausanne, Switzerland.

Manuscript submitted August 14, 1989.

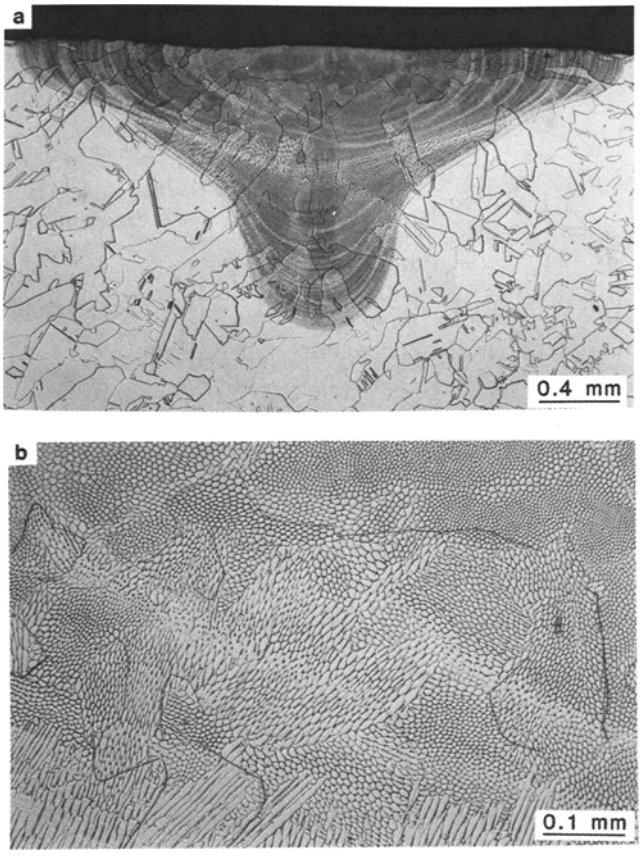

Fig. 1—Transverse-section micrographs at (*a*) low and (*b*) high magnification of a polycrystalline Fe-15Ni-15Cr weld made at 4.2 mm/s.

shape that is readily available after welding polycrystalline materials is the outermost size and shape of the pool as defined by the fusion line and observed in a transverse view. Discontinuities in microstructural features due to changes in the solidification velocity can sometimes be observed in the form of striations. While these striations may provide some information on the 3-D shape of the weld pool, they are often obscured by the polycrystalline microstructure, as shown in Figure 1. Consequently, no detailed information on the 3-D nature of the weld pool can be directly obtained from such polycrystalline welds.

The situation for welds made with single crystals is quite different from that described above. In well-characterized single crystals, significantly more information concerning the weld pool shape and overall microstructural development can be obtained. A few preliminary attempts have been made previously to characterize the development of the fusion-zone structure using single or coarse-grained crystals.[1,2,8,9] More recently, however, detailed studies[10,11] of the microstructural development in a pure, well-characterized autogenously welded single-crystal Fe-15Ni-15Cr alloy have been carried out, and the results have been analyzed with respect to growth crystallography. In this more recent work, a 3-D geometric analysis was developed in which the relationships between the velocities of the moving heat source, $\vec{v}_b$, the solidification front, $\vec{v}_s$, and the dendrite tip, $\vec{v}_{hkl}$, were derived. With the assumption of a steady-state constant pool shape, these relationships show that at any given location on the melt pool interface,

$$|\vec{v}_{hkl}| = |\vec{v}_b| \cos\theta/\cos\psi \qquad [1]$$

where θ is the angle between $\vec{v}_b$ and $\vec{v}_s$ and ψ is the angle between $\vec{v}_{hkl}$ and $\vec{v}_s$, as shown in Figure 2. Since the direction of $\vec{v}_s$ is given by the normal, $\vec{n}$, to the melt pool interface, the velocity of the dendrite trunks is influenced by the melt pool shape. Selection of the one [*hkl*] dendrite trunk growth direction among the six ⟨100⟩ easy growth directions was then determined according to a minimum velocity (equivalent to a minimum undercooling) criterion. This selection criterion corresponds to choosing the dendrite growth direction that has the best alignment with the heat flow direction.

The specific, active dendrite growth directions were determined in Reference 10 as a function of the solidification front orientation for different crystal orientations, namely, welds made along either the [100] or [110] crystallographic directions on a (001) surface. Subsequently, the analysis was extended to include other welding orientations, namely, a (110) surface with welds along [001], [1$\bar{1}$0], or [1$\bar{1}$1] directions and a (111) surface with a [1$\bar{1}$0] weld direction.[11] An analysis for any general crystal orientation was also presented.[11] Since there is only one set of crystallographic axes in a single-crystal weld, the transitions in dendritic structure from one growth direction to another can be directly associated with specific values of θ and ϕ that describe the 3-D orientation of the solidification front normal (Figure 2). Therefore, information on the 3-D weld pool shape can be obtained from the examination of single-crystal weld microstructures.

The present paper extends the results of the previous

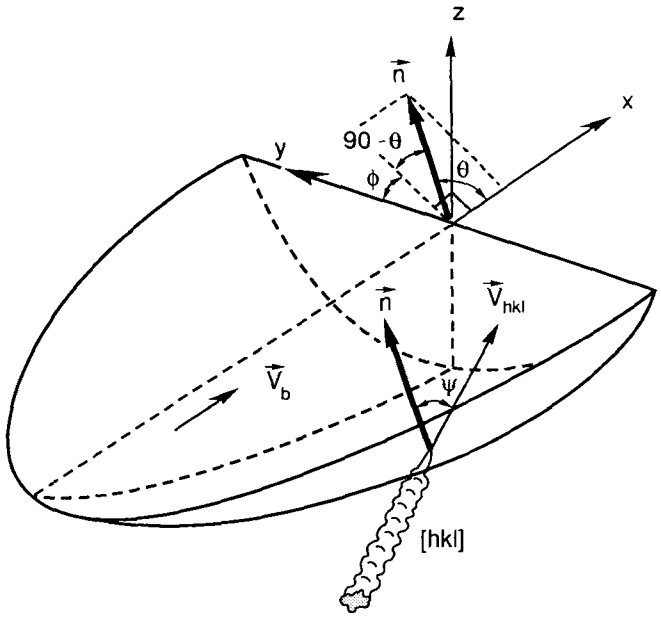

Fig. 2—Schematic representation of the melt pool interface showing the normal to the melt pool interface, $\vec{n}$, the velocity, $\vec{v}_b$, of the moving heat source, and the velocity, $\vec{v}_{hkl}$, of one dendrite trunk variant. Also shown are the three angles θ, ϕ, and ψ that are used to define the weld pool and dendrite orientations.

investigations.[10,11] Additional details regarding the determination of weld pool shapes and dendrite growth directions as a function of welding speed are examined. In addition, several controlled conditions that relate to more realistic and practical welding situations than were examined in the earlier work by the authors are considered. These include overlapping multipass autogenous welds and butt welds of two single crystals with different orientations. The present work emphasizes the role of pool shape on the microstructural development, and the experimental results are discussed in light of the detailed dendrite growth analysis made previously.[10,11]

II. EXPERIMENTAL PROCEDURE

The experimental procedure used to grow the Fe-15Ni-15Cr single crystals employed in this study is described in detail elsewhere.[10] Single-crystal specimens used in making the full-penetration welds were in the form of disks approximately 1.5 cm in diameter and 0.3-cm thick. These disks were cut from the as-grown single crystal using electric spark erosion and were subsequently mechanically polished and then electropolished. Before sectioning from the as-grown crystal, the specimens were carefully oriented by means of the Laue back-reflection X-ray technique so that the surface of the disk corresponded to a (001) crystallographic plane. In addition, [110] and [100] directions lying in the plane of the disk were identified from Laue back-reflection photographs and marked so that welds could be made along these predetermined directions.

All electron beam welds were made in a horizontal position with a 15 kW Leybold Heraeus electron beam welder at 100 kV accelerating voltage and 5 to 7 mA beam current. Single-pass welds were made along [100] and [110] directions at welding speeds ranging from 3 to 42 mm/s. Autogenous overlapping multipass welds were made on crystals with a (001) surface along the [100] direction at 4.2 mm/s. Butt welds were made along the interface between two single crystals having the same (001) surface orientation but with different directions parallel to the interface (and beam) direction (*i.e.*, [110] for crystal A and [100] for crystal B). Figure 3 shows the joint geometries and designs used for making all of the welds.

Detailed microstructural analysis was performed using conventional metallographic techniques after carefully sectioning the specimens. The specimens were electrolytically etched at 0.1 A and 3 V for 20 seconds in a 10 pct solution of oxalic acid in water.

III. RESULTS AND DISCUSSION

A. *Relationship between Three-Dimensional Weld Pool Shape and Transverse-Section Micrographs*

If it is assumed that the shape of the weld pool remains constant during the welding of single crystals, then information on the 3-D nature of the weld pool can be extracted from two-dimensional (2-D) micrographs. The correlation between the 3-D weld pool shape and the

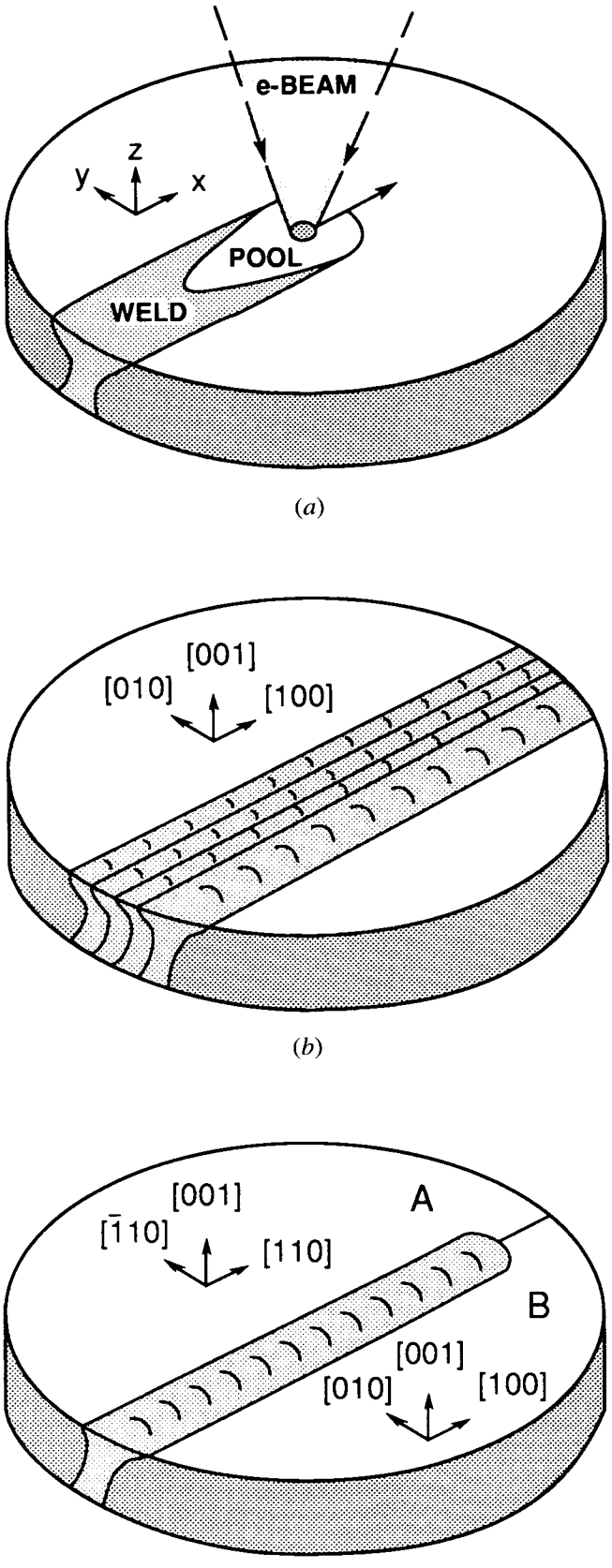

Fig. 3—Welding configurations used in the present study: (*a*) autogenous single-pass single-crystal weld, (*b*) autogenous multipass single-crystal weld, and (*c*) autogenous bicrystal weld.

2-D features observed in a transverse micrograph can be understood with the help of Figure 4. The weld pool interface in the three planes A, B, and C in Figure 4(a) corresponds to the contour lines A′, B′, and C′ in the projection of the weld pool seen in Figure 4(b).* Outlines of the fusion-zone boundary such as B′ and C′, lying within the outermost fusion zone line A′, are often readily visible in micrographs as a result of the natural fluctuations and oscillations that are present in the weld pool during solidification. By defining the orientation of the weld pool surface in terms of the angles θ and ϕ (Figure 2), which vary continuously throughout the weld pool, some specific locations along the surface of the weld where θ and ϕ are known can be identified in a transverse-view micrograph. In a transverse view of the weld, θ is equal to 90 deg along the outer trace (A′ in Figure 4(b)), whereas within the weld, $\theta \leq 90$ deg. The values of ϕ along the outer weld pool trace can be determined directly, as shown in Figure 4(b). In addition, along the weld centerline, ϕ must be equal to 90 deg as long as the weld pool shape is symmetrical. Furthermore, wherever fusion-zone outlines such as B′ and C′ are evident in the microstructure, ϕ can be determined in a transverse micrograph in a fashion similar to that shown in Figure 4(b).

*It is assumed that the locus of points that define the widest section of the fusion zone lie in a transverse plane perpendicular to the x-axis (Figure 2).

Two schematic weld pool shapes, based on the weld pool shape analysis developed in Reference 10, are shown in Figures 4(c) and (d). At low welding speeds (Figure 4(c)), the length of the pool along the welding direction is rather short, and the angle θ along the weld pool centerline is close to 0 deg near the top and bottom of the weld. Increasing the welding speed (Figure 4(d)) produces a more elongated weld pool, and the θ angle characterizing the normal, $\vec{n}$, is large for a much greater section of the weld pool surface. Based on an evaluation of the microstructures in single-crystal welds, characteristics of the weld pool shape, such as those shown in Figures 4(c) and (d) can be determined.

The specific dendrite orientations that are expected as a function of θ and ϕ have been calculated for several

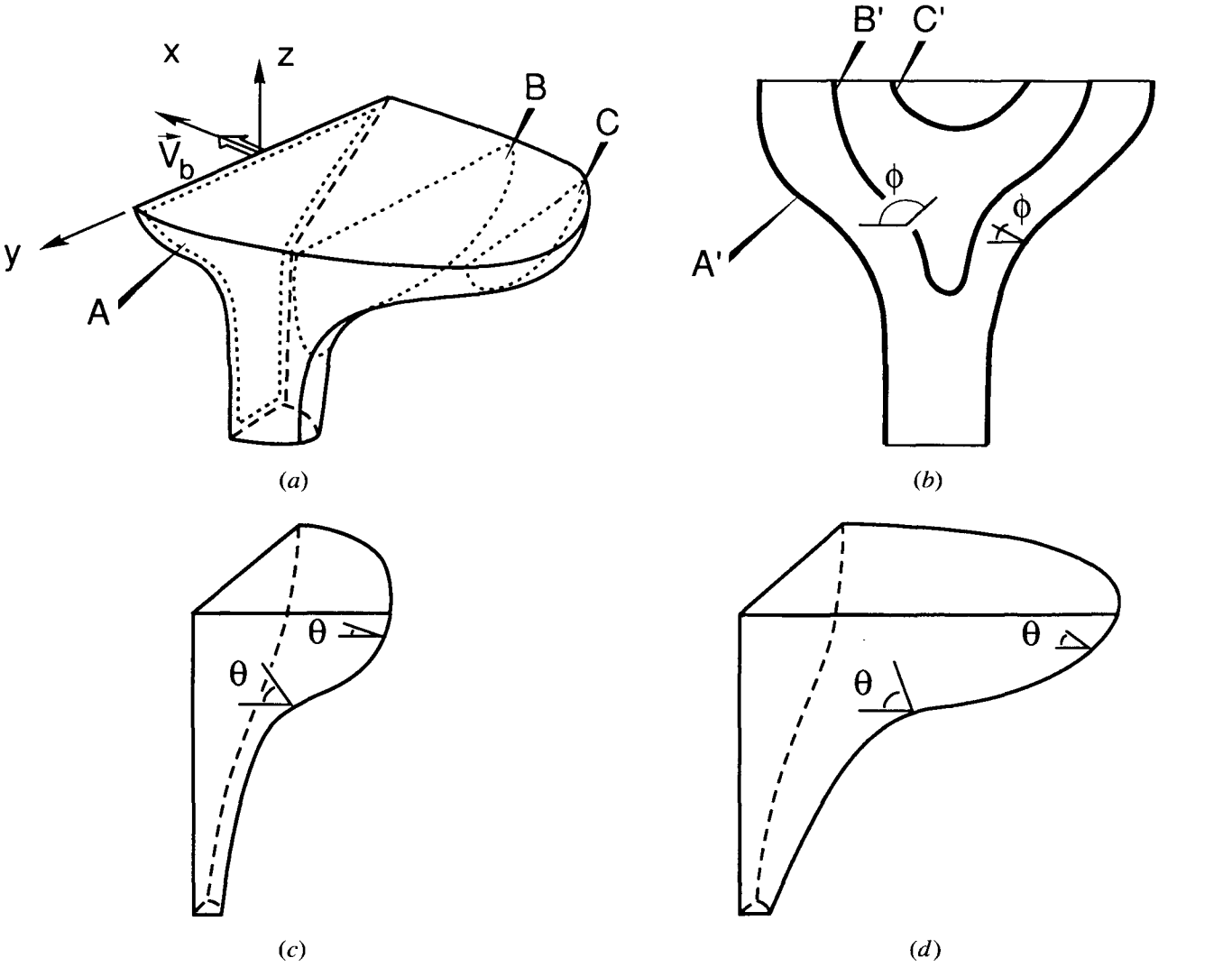

Fig. 4—Schematic representation of (*a*) 3-D electron beam weld pool, (*b*) transverse section of the solidified melt pool showing three contours that correspond to the weld pool surface in three different planes across the weld pool in (a), (*c*) schematic 3-D pool shape at low welding speed, and (*d*) schematic 3-D pool shape at high welding speed.

crystal orientations.[10,11] The results for welds on a (001) surface in either the [110] or [100] directions are reproduced in Figure 5 to provide a basis for the evaluation and interpretation of the present experimental results. By examining the dendrite trunk orientations found in single-crystal welds and comparing the results with those predicted, useful information regarding the 3-D melt pool shape can be obtained. In particular, where there are transitions from one dendrite trunk orientation to another, specific values of θ and ϕ can be assigned to these locations by referring to the diagrams shown in Figure 5.

B. *Effect of Welding Speed and Weld Direction*

Figures 6 and 7 show the macrostructures and microstructures of two welds made along the [110] direction on single crystals with (001) surfaces at welding speeds of 4.2 and 42 mm/s, respectively. As noted previously,[10] Fe-15Ni-15Cr dendrites are approximately cylindrical in shape and generally do not show any branching except in a few locations. In the micrographs, the dendrites appear either as elongated cells when cut approximately parallel to their trunk direction or as circles or ellipses when cut nearly normal to their trunks. The cellular appearance of these dendrites is associated with the low degree of segregation of Cr and Ni in this system, together with the rather large thermal gradient encountered in welding. They clearly behave as dendrites, however, since they definitely grow along the ⟨100⟩ crystallographic directions, as shown in Figures 6 and 7. Some branching is evident in the microstructures, particularly in the vicinity of transitions from one trunk orientation to another (see lower portion of Figure 6(b) and center region of Figure 7(c)). Branching in the region of transitions between trunk orientations may simply indicate that the preference or driving force for the selection of one trunk growth orientation with respect to another is minimal. In addition, it is likely that branching is the mechanism by which new trunk growth directions develop from existing dendrites.

At a low welding speed of 4.2 mm/s, the microstructure of the fusion zone is dominated by dendrites growing along [100] and [010] directions, and these dendrites are well oriented, as evident from the symmetry

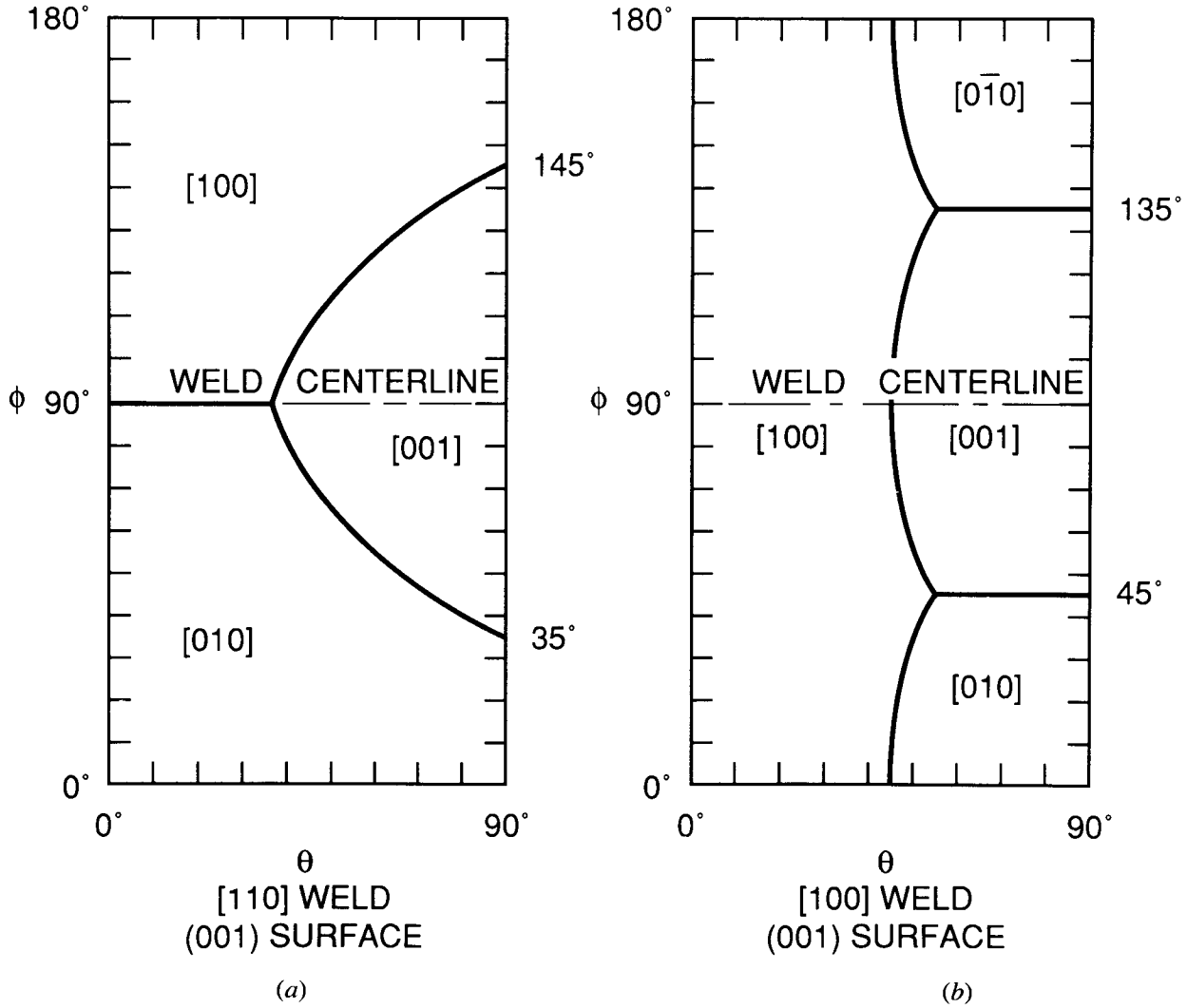

Fig. 5—Dendrite growth orientation selection diagrams showing the preferred dendrite growth directions as a function of the angles θ and ϕ which describe the solidification front orientation. ϕ = 90 deg corresponds to the weld centerline, whereas θ = 90 deg corresponds to the outer weld trace as seen in a transverse section. (*a*) [110] weld direction on a (001) surface, and (*b*) [100] weld direction on a (001) surface.

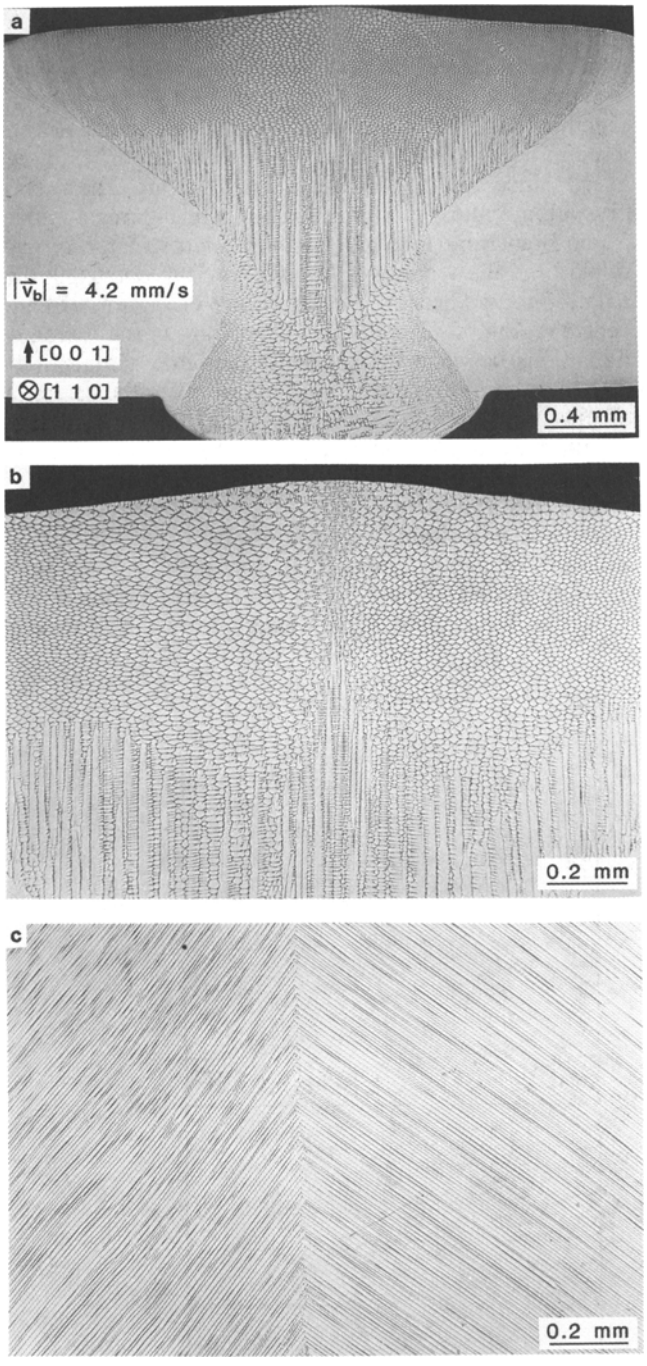

Fig. 6—Structure of a single-crystal weld made at 4.2 mm/s along a [110] direction on a (001) surface. (*a*) Transverse macroscopic view, (*b*) higher magnification of (a), near the top of the weld, and (*c*) top view of microstructure. Weld direction in (c) is from the bottom to the top.

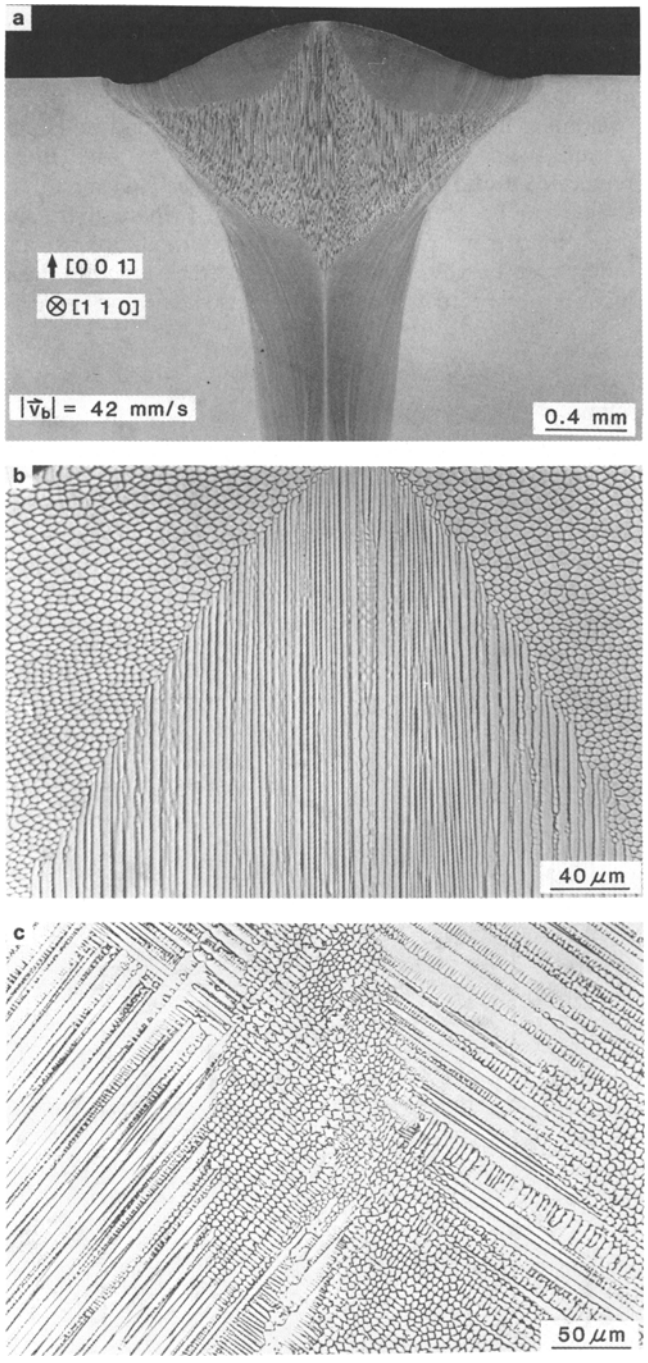

Fig. 7—Structure of a single-crystal weld made at 42 mm/s along a [110] direction on a (001) surface. (*a*) Transverse macroscopic view, (*b*) higher magnification of (a), near the top of the weld, and (*c*) top view of microstructure. Weld direction in (c) is from the bottom to the top.

of the micrographs in Figures 6(b) and (c). By referring to the dendrite growth selection diagram shown in Figure 5(a) for welds in the [110] direction, the fact that [001] dendrites are found in the center section of the weld (including the centerline where ϕ = 90 deg) indicates that θ must be larger than 35 deg in this limited central region but smaller than 35 deg near the top and bottom of the weld. Therefore, in the longitudinal plane along the centerline (x-z plane in Figure 2), the center of the weld pool interface must be flatter over a short distance where θ is greater than 35 deg, resulting in a plateau-like section, as shown schematically in Figure 4(c). However, since the [001] dendrites tend to be branched, it is likely that this plateau region does not approach the horizontal and that θ is not much larger than 35 deg along the weld centerline. Since the region where [001] growth is found is restricted, it can be concluded that the weld pool is short in length, as shown in Figure 4(c).

At the higher welding speed of 42 mm/s, as shown

in Figure 7(a), the microstructural features within the weld metal are distinctly different from those for welds made at a low welding speed. First, the overall weld profile is narrower, with a less well-defined crown at the top of the weld. Second, the region of growth of [001] dendrites is significantly larger than in the slower weld and extends to the top surface. In addition, the growth of [100] and [010] dendrites in the bottom half of the weld pool is much more uniform, and each zone is more sharply defined. Throughout the weld, the tendency for branching is reduced. All of these factors, when considered in light of the dendrite selection diagram in Figure 5(a), are consistent and suggest that the weld pool is more extended, with a better defined and flatter plateau region along the centerline as viewed in the longitudinal plane. The pool shape that is inferred from these results resembles that shown schematically in Figure 4(d).

The tendency for branching of the dendrites may also be related to the thermal gradient at the weld pool interface. Although the thermal gradient and the weld pool shape are not independent of one another but are, in fact, strongly interrelated, an examination of the effect of thermal gradients provides an alternative point of view for studying and evaluating the microstructural development within the weld pool. Near the center of the welds (or at low welding speeds), the expected thermal gradient is lower than near the outer edge of the weld (or at high speeds). If the gradient is small, then more heavily branched dendrites are expected. The net result should be that the transition from one dendrite growth direction to another is more diffuse. With higher thermal gradients, dendrites are less branched, and transitions from one growth direction to another are sharper. The experimental observations agree with these expected results since the transitions between different dendrite growth regions are sharp, with little branching evident, at the higher welding speed. Such relatively sharp transitions from one dendrite orientation to another were also found in earlier work on textured polycrystalline silicon-iron sheet.[1]

Figures 8 through 10 show the macrostructures and microstructures of three welds made along the [100] direction on single crystals with (001) surfaces at welding speeds of 3, 4.2, and 42 mm/s, respectively. The microstructure of the low-speed (3 mm/s) weld in this orientation consists of dendrites with three different orientations. These regions can be clearly seen in Figure 8(a) marked "A," "B," and "C." In those regions marked A, [100] dendrites are present, while those marked B contain [010] or [0$\bar{1}$0] dendrites, and region C is characterized by [001] dendrites. As for the case of [110] welds, the presence of these different regions with different dendrite growth directions can be directly attributed to, and correlated with, the weld pool shape. In the A regions where [100] dendrites exist, θ must be small (<45 deg; see Figure 5(b)), and therefore, the solidification front must be close to perpendicular to the welding direction. As found for the low-speed [110] welds, the presence of [001] dendrites in the central region of the weld indicates that the weld must have a limited plateau region. Thus, the weld pool shape must be similar to that shown in Figure 4(c).

The change in general outer pool shape with welding speed for [100] welds is similar to the trend found for [110] welds. The distinct crown at the top of the weld becomes smaller and the pool becomes more slender at the highest welding speed. In fact, for welds made at the same speed but in different crystallographic directions, the pool shapes are quite similar (compare Figures 6 and 9, and 7 and 10). Thus, the weld pool shape is not influenced by the crystallographic orientation. This result is expected since the weld pool shape is determined by

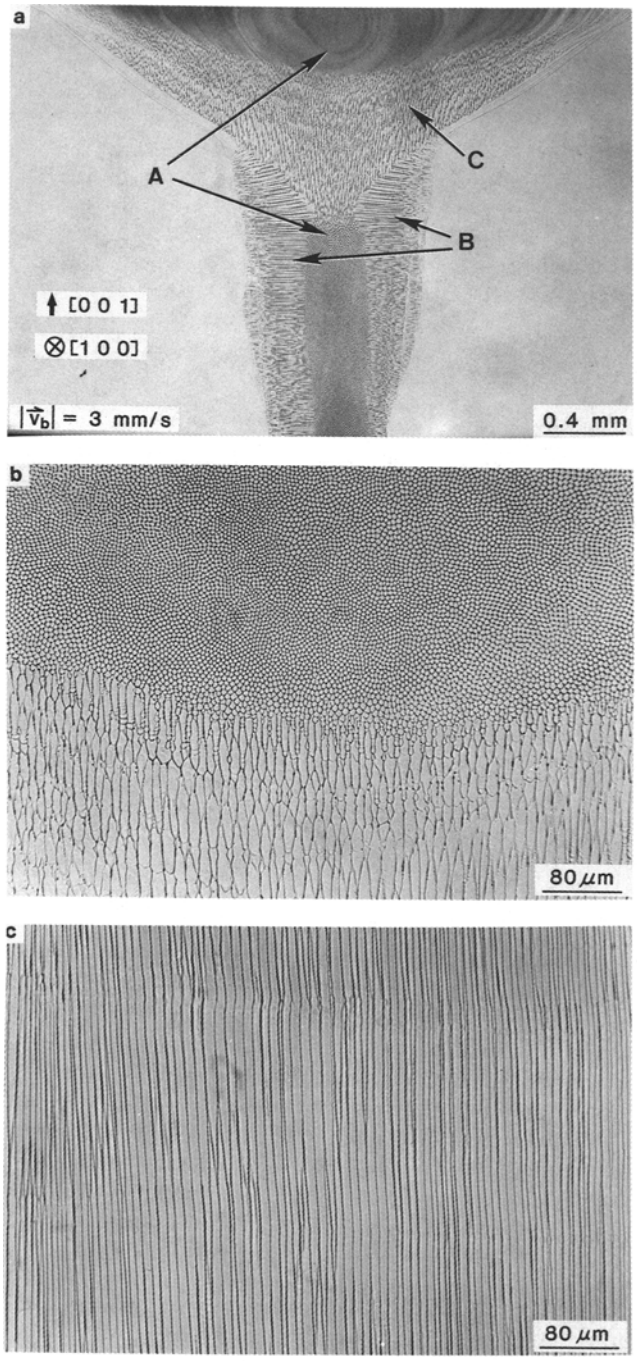

Fig. 8—Structure of a single-crystal weld made at 3 mm/s along a [100] direction on a (001) surface. (*a*) Transverse macroscopic view, (*b*) higher magnification of (a), near the top of the weld, and (*c*) top view of microstructure. Weld direction in (c) is from the bottom to the top. Three different dendritic orientations, as described in Section III–B, are labeled "A," "B," and "C."

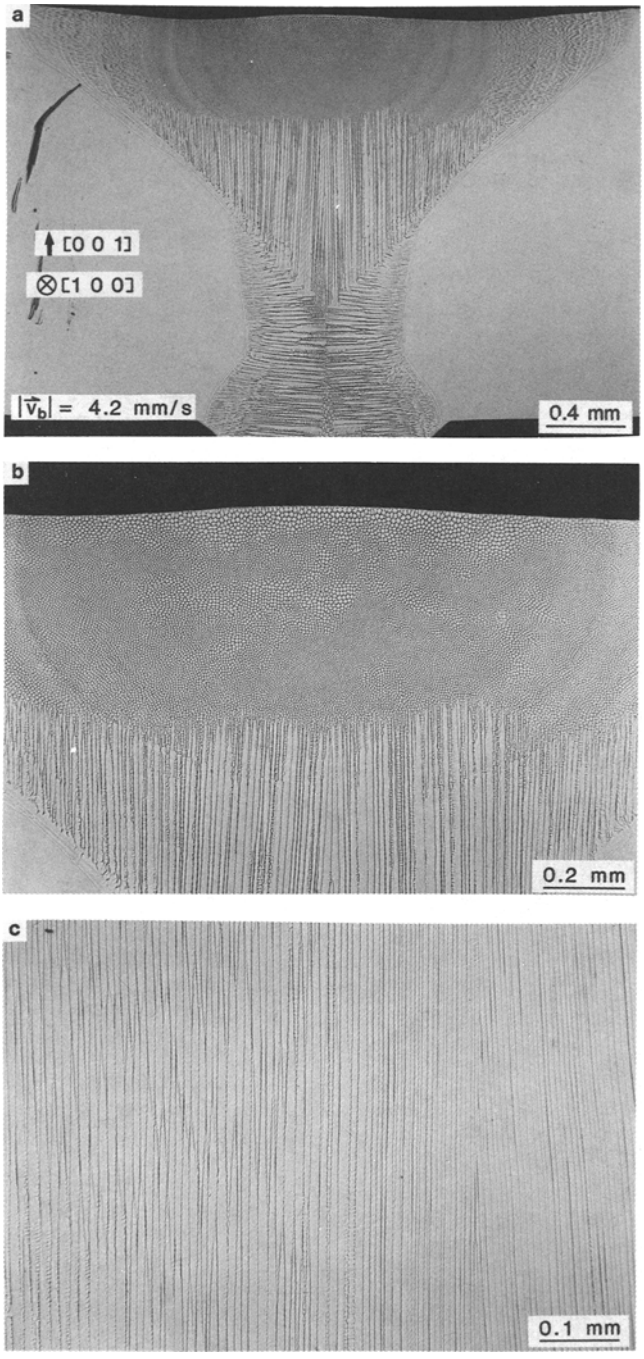

Fig. 9—Structure of a single-crystal weld made at 4.2 mm/s along a [100] direction on a (001) surface. (*a*) Transverse macroscopic view, (*b*) higher magnification of (a), near the top of the weld, and (*c*) top view of microstructure. Weld direction in (c) is from the bottom to the top.

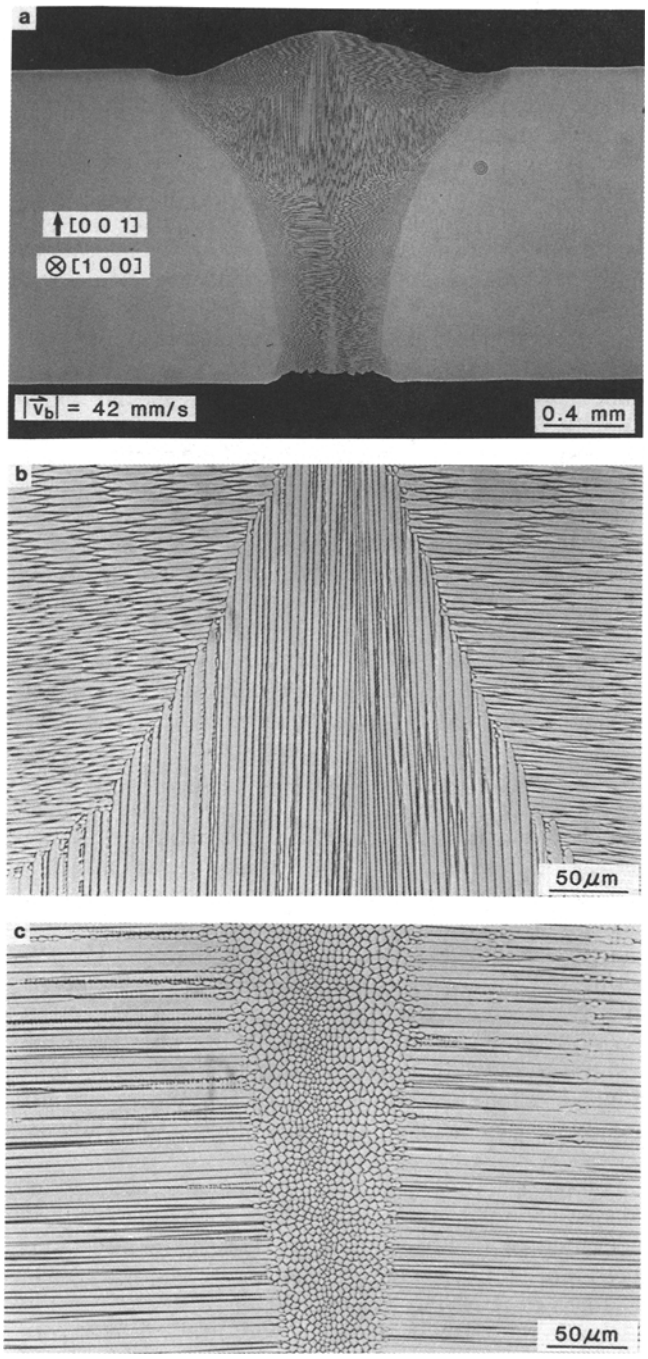

Fig. 10—Structure of a single-crystal weld made at 42 mm/s along a [100] direction on a (001) surface. (*a*) Transverse macroscopic view, (*b*) higher magnification of (a), near the top of the weld, and (*c*) top view of microstructure.

the material's thermal diffusivity, which is essentially isotropic in the alloy examined here. The conclusion that the weld pool shape is independent of the crystal orientation is supported by the similar shape and size of the [001] dendritic growth zones in comparable [100] and [110] welds. As seen in Figure 5, the stability ranges for [001] dendrites in terms of θ and ϕ are comparable for welds made in both directions. Therefore, if the regions in which these [001] dendrites are found are similar, then it must also be true that the weld pool shapes that determine the size and shape of these regions must be similar.

As the welding speed is increased above 3 mm/s, the lower zone with [100] dendrites is replaced by [010]/[0$\bar{1}$0] dendrites. By referring to Figure 5(b), θ must be greater than approximately 45 to 50 deg in this lower section of the weld, while ϕ must change rapidly from <45 to >135 deg in crossing the centerline from right to left. These two requirements indicate that the weld

pool near the bottom is not gently curved around the centerline but rather must be more angular. Based on the conclusion that the weld pool shape does not change with the crystallographic direction of the weld, this same angular shape near the bottom of the pool is expected in the [110] weld as well. It is interesting to note that this deduction could not have been made from the results of the [110] welds alone since the range of stability of the [100]/[010] dendrites at low or high ϕ values spans the entire range of θ from 0 to 90 deg. Furthermore, as the welding speed is increased from 4.2 to 42 mm/s, the [100] dendrites near the top of the weld are replaced by [010]/[0$\bar{1}$0] and [001] dendrites. This is the same effect that was observed for the [110] welds—namely, the pool becomes more elongated in the welding direction, and its shape resembles that illustrated in Figure 4(d). The generality of these results is, of course, dependent upon the reproducibility of the weld pool shape from weld to weld. Irregularities due to convection, weld condition fluctuations, and random nucleation may exist to some extent, thereby altering the weld pool shape and resultant dendritic growth patterns.

Another interesting feature of the present results is the apparent bending of dendrites that is occasionally observed. Examples of this bending can be found in Figures 8(a) and 9(a) in the center of the welds near the transition between the [010]/[0$\bar{1}$0] and [001] dendrites. In Figure 9(a), both the [010]/[0$\bar{1}$0] and the [001] dendrites appear to be curved. It is clear from the micrographs that the "bent" dendrites belong to the same single-crystal orientation as the other dendrites. The redirection of these dendrites may be due to convection effects since it is possible that convection within the weld pool preferentially melts one side of the growing dendrites so that they appear to bend in the opposite direction. Alternatively, convection may actually lead to physical deformation of the dendrites. Such deformation, if prevalent to a larger extent, might eventually lead to dendritic detachment and equiaxed growth.

Finally, some evidence of branching is also found in the [100] welds—once again in the regions of transition from one dendrite growth direction to another. The branching is most clearly seen near the bottom of the 4.2 mm/s weld. This is the same area in which branching was found in the [110] welds. Branching in this area of the weld is not seen in the 3 mm/s weld, indicating that the solidification front orientation is well within the stability range for [100] dendrites in this latter case.

All of the microstructural variations described above are the result of variations in the pool shape, which is determined by the welding parameters. The analysis of dendrite growth selection, based on the optimum alignment of dendrites with the solidification front normal (*i.e.*, growth at a minimum velocity/undercooling), allows for a qualitative evaluation of the 3-D pool shape from 2-D transverse-view micrographs. Since the pool shape is not influenced by the welding direction, microstructural information from welds made in different crystallographic directions can be combined to provide a more precise and complete picture of the actual weld pool shape. Furthermore, as noted, these results provide the necessary basis for understanding microstructural formation and grain growth selection in polycrystalline specimens.

C. *Overlapping Multipass Welds*

Figure 11 shows two transverse-view macrographs of overlapping welds made on separate samples. The welding conditions for each sample were similar: *i.e.*, the welds were made at 4.2 mm/s in the [100] direction on crystals with (001) surfaces. Figures 12(a) and (b) show higher magnification photomicrographs of the welds in Figure 11 in transverse- and top-section views, respectively. Figures 11 and 12 show remarkable reproducibility from pass to pass and from sample to sample of both the overall weld profile and the dendritic growth patterns. As described in detail in the previous section, the dendritic growth patterns are related to the 3-D weld pool shapes so that the similarity in dendritic patterns indicates that the weld pool shapes must have been essentially identical in successive passes. The weld shapes, with their noticeable crowns at the top, and the dendritic patterns within each weld pass more closely resemble the 3 mm/s single-pass welds than the 4.2 mm/s single-pass welds (Figures 8 and 9, respectively). This difference may be due to the fact that the multipass welds were not

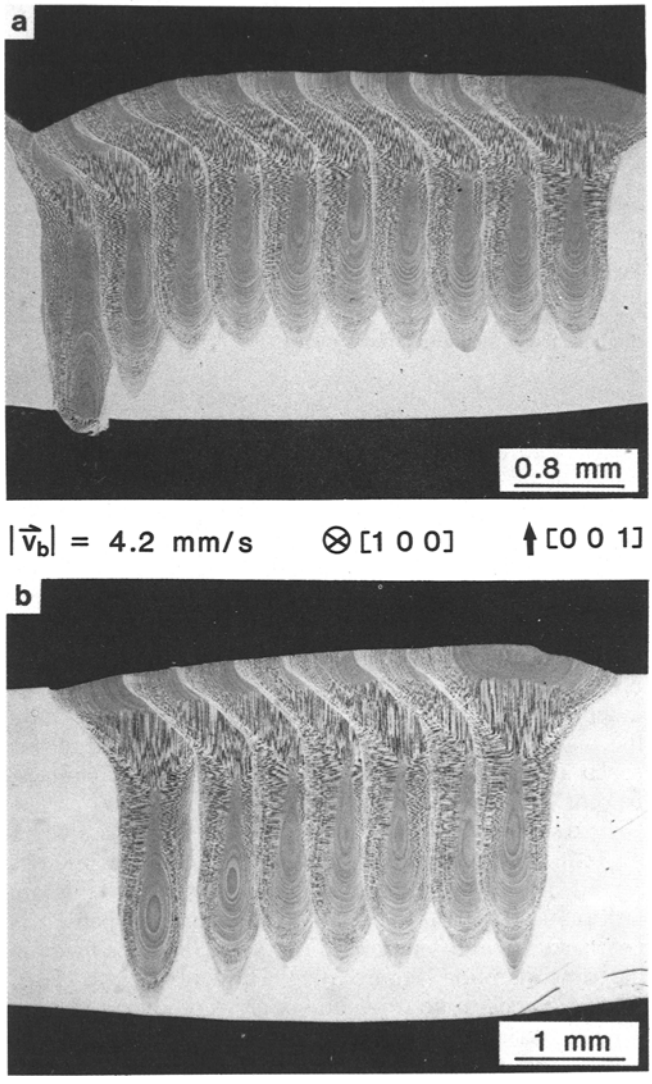

Fig. 11—Transverse sections of two separate multipass overlapping welds made on a single crystal of Fe-15Ni-15Cr at 4.2 mm/s along a [100] direction and on a (001) surface.

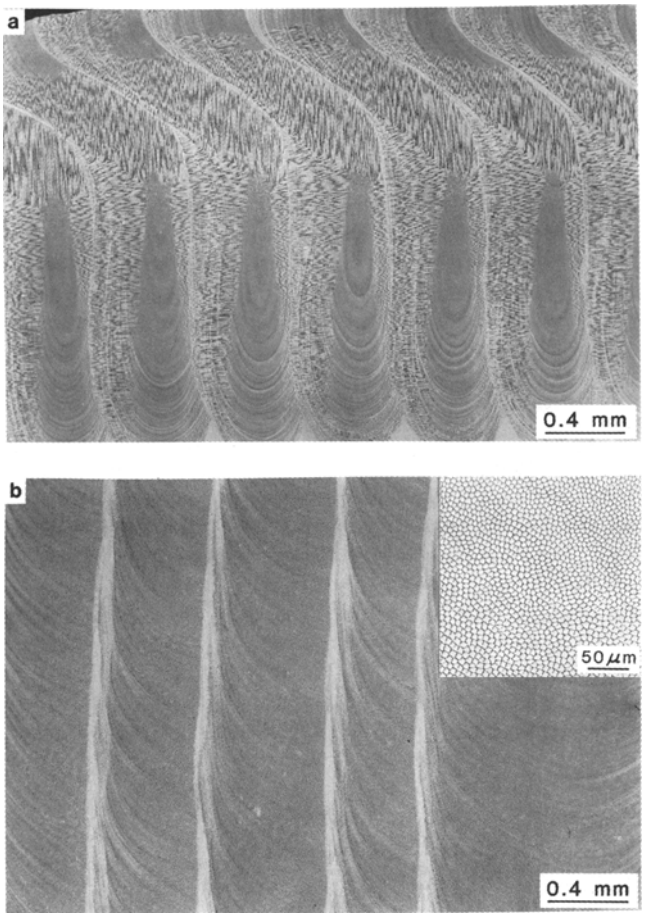

Fig. 12—(*a*) Higher magnification transverse section of the weld shown in Fig. 11(a) and (*b*) higher magnification top-section micrograph of the multipass weld shown in Fig. 11(b). Magnified insert in (b) shows the honeycomb dendritic arrangement.

fully penetrating welds (in contrast to the single-pass welds) and that this difference resulted in a slight alteration of the heat flow and subsequent weld pool shape. It is also possible that during the multipass welding, the overall specimen temperature was elevated, and as a result, the heat flow was affected. If the specimen temperature was raised significantly, the net effect on the heat flow should be the same as that associated with welding at a lower speed. The results show that the shape of the crown and the interior dendritic pattern are not independent in that the multipass welds did not exhibit the outer weld shape of single-pass welds made at one speed and the inner dendritic growth patterns characteristic of another welding speed.

As discussed previously for low-speed single-pass welds made in the [100] direction on a (001) surface, the observed dendrite orientations in the multipass welds are [100], [010]/[0$\bar{1}$0], and [001]. The dendritic pattern is nearly identical to that found for 3 mm/s welds made in the same direction (Figure 8). As shown in Figure 12(a), the various dendrite orientations are reproduced in each of the overlapping welds from the fusion line inward, irrespective of the dendrite orientation present at the fusion line from the previous pass. The observed behavior is exactly as if each welding pass erases the previously developed microstructure but retains the crystallographic nature of the single-crystal base material. All of these observations agree very well with the theoretical predictions and experimental observations described previously.[10,11] Figure 12(b) shows the microstructural features on the top surface of the overlapping welds. The microstructure in Figure 12(b) consists exclusively of [001] dendrites appearing as small circles arranged in a honeycomb structure. This result is contrary to what was observed in Figure 9(c) but is readily explained: *i.e.*, the [001] dendrites seen in the top-view micrograph of Figure 12(b) are present because the metallographic section was polished at some distance below the top surface since the top surface of the multipass weld was uneven (Figure 11). Therefore, the section has cut the [001] dendrites growing upward underneath the original top surface (Figures 11 and 12(a)).

Several other interesting features are associated with the dendrite growth patterns observed in the multipass weld. Figure 13 is a high-magnification view of one of the passes in the weld of Figure 11(a). The micrograph shows the tendency for branching in the vicinity of the transitions from one dendrite growth direction to another, as discussed earlier. However, this micrograph also shows the mechanism by which new growth directions develop. In the areas marked "A," the [0$\bar{1}$0]/[010] dendrites show signs of branching that eventually lead to the growth of [001] dendrites from these branches. Thus, when the orientation of the solidification front is correct, the branches develop into primary dendrites and form a new zone with a different primary growth direction. As the stability of these dendrites with respect to the precursors increases (*i.e.*, as the solidification front orientation moves away from the critical orientation delineated by the transition lines in Figure 5), these new dendrites become more cylindrical in shape, and any signs of branching are lost. Evidence of a similar transition from [100] dendrites to [001] dendrites can also be seen in Figure 13 (area marked "B"). The circular cross section of the [100] dendrites becomes more elongated in the [001] direction until eventually the [001] dendrites take over in the form of elongated cells. It is also clear from these micrographs that the transitions between various trunk orientations occur over a range of the angles θ and

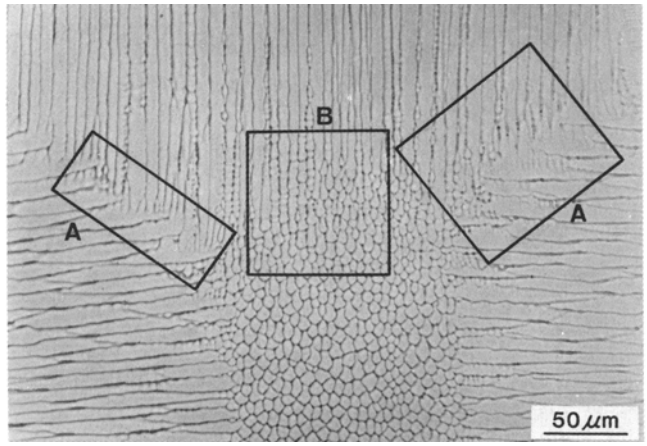

Fig. 13—Transverse-section micrograph of Fig. 11(a) showing the branching mechanism that produces [001] dendrite trunks from the branches of [010]/[0$\bar{1}$0] (area "A") or [100] (area "B") dendrites.

ϕ, rather than for a specific orientation of the weld pool surface normal.

Transitions between dendrite trunk orientations may also be influenced by irregularities and disturbances in the weld pool. As can be seen in the transverse micrograph shown in Figure 14, the growth of [010] dendrites near the top of the weld is not very regular. For the weld pass labeled "A," [010] dendrites are growing from the left side of the pool, as predicted from the geometrical analysis[10] and the dendrite growth selection diagram in Figure 5. However, the same location in the pool in the weld traces "B" and "C" exhibits a mixture of [010] and [100] dendrite trunk orientations. Thus, the assumption of a constant pool shape is apparently not totally valid here, and the weld pool irregularities are sufficiently large to influence the dendrite selection process. Since this alteration is in the vicinity of the transition from one orientation to another, a small deviation in pool shape is certainly enough to accomplish this change in trunk orientation. The influence of melt pool disturbances on dendrite selection is mainly observed near the outer trace of the weld pool. The growth directions of the dendrites, however, remain along ⟨100⟩ regardless of the melt pool fluctuations. Once again, this clearly shows that the growth direction of the dendrites seen in these micrographs is along the easy growth directions and not along the heat flow direction.

Another interesting feature associated with the overlapping weld passes is the occurrence of elliptical striations in the bottom half of the weld where [100] dendrites grow (Figure 15). Although the contrast varies around these ellipses, the [100] dendritic structure is quite uniform in size, as expected, since these dendrites all grow with the same velocity.[10] The average trunk spacing measured inside the ellipse is 2.1 μm, whereas, outside the center ellipse, the trunk spacing is 2.4 μm. The existence of these elliptical striations and their implications for the weld pool shape are noteworthy. Since these striations result from oscillations within the weld pool and, therefore, outline the instantaneous melt pool position, the existence of closed loops means that the 3-D pool shape has a protrusion at the rear of the pool. This effect is shown schematically in Figure 16(a). Such elliptical striation patterns were not found in the fully penetrating single-pass welds and were even absent in most of the passes in the multipass weld shown in Figure 11(a). Presumably this protrusion is due to the heat and fluid flows patterns that are present during welding. Although it is not exactly the same effect, evidence for a similar broadening of the pool at the bottom is also found for the single-pass welds. The full-penetration welds shown in Figures 6(a), 9(a), and 10(a), and even the first pass in Figure 11(a), show striations near the bottom that are concave downward. Such striations imply that the weld pool becomes larger at the bottom. The weld pool shape with such an expanded lower section is drawn schematically in Figure 16(b). The assumption of a broader weld base is supported by the fact that the outer weld trace in these welds also broadens. Although these details on the weld pool shape are difficult to verify directly, it would be quite interesting to model mathematically the weld pool shapes in order to determine if these unusual features based on experimental observations can be duplicated by modeling.

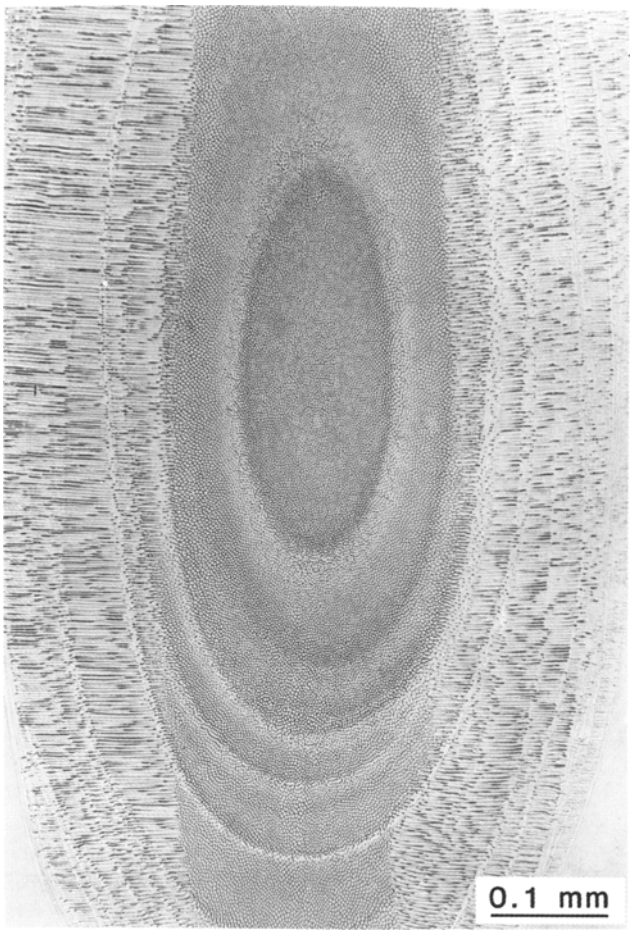

Fig. 15—Enlargement of the bottom of one of the passes in the weld shown in Fig. 11(b) showing the elliptical striations that correspond to a protrusion in the weld pool surface.

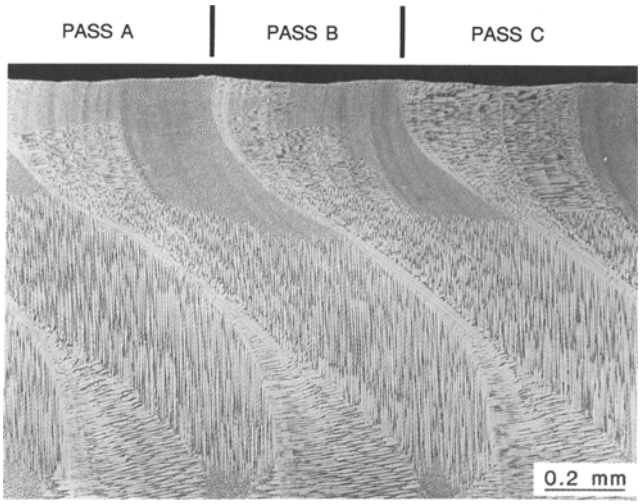

Fig. 14—Enlarged transverse view of the multipass weld shown in Figs. 11(a) and 12(a) showing the irregular growth of [010] dendrites near the top surface in three successive passes A, B, and C.

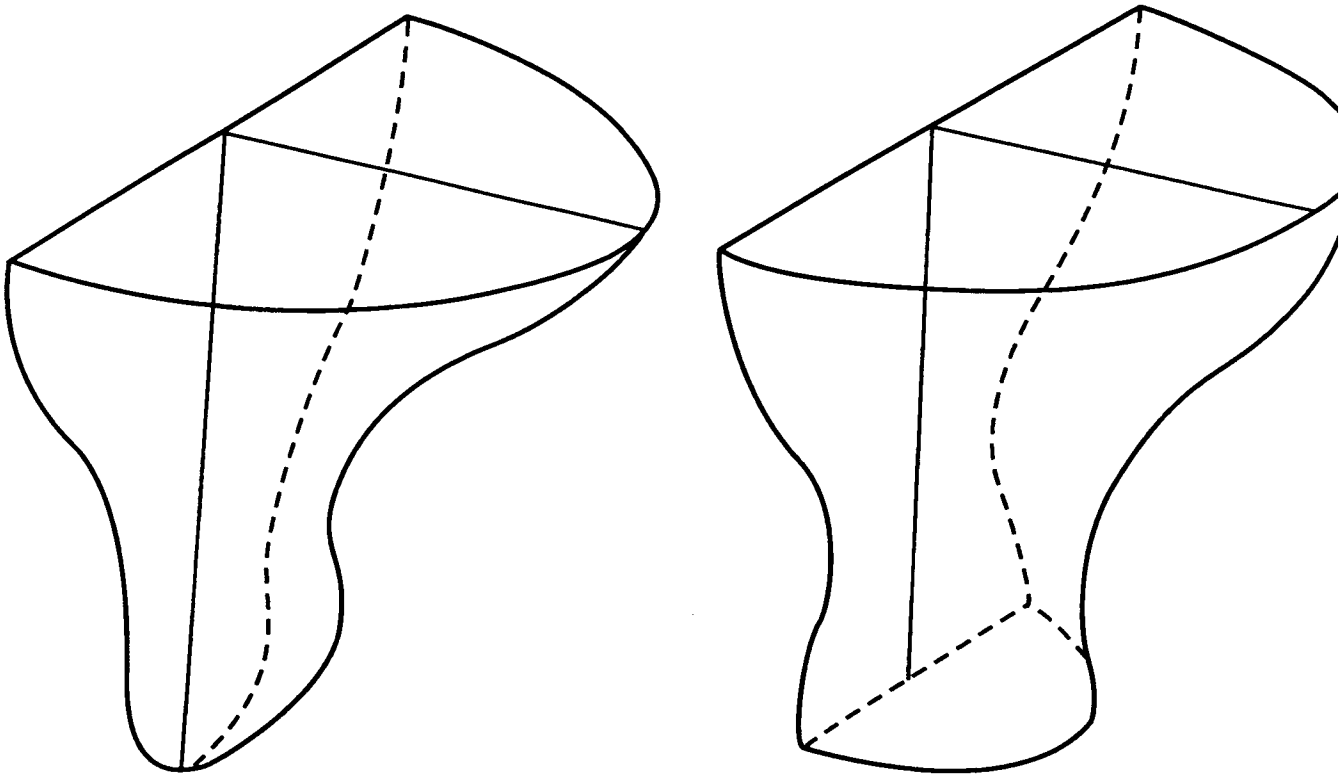

(*a*) (*b*)

Fig. 16—Schematic representation of the 3-D electron beam weld pool shapes: (*a*) partial-penetration weldment with a protrusion near the botto of the weld and (*b*) full-penetration weld showing an enlarged weld pool at the bottom.

D. *[110] and [100] Butt Welds*

Figure 17 shows a transverse-section photomicrograph of the butt weld of two crystals, A and B, joined in such a way that the welding direction and joint interface were parallel to $[110]_A$ and $[100]_B$. For both crystals, the top surface is (001), and the weld was made at 8.3 mm/s. The outer weld shape, with a modest crown at the top,

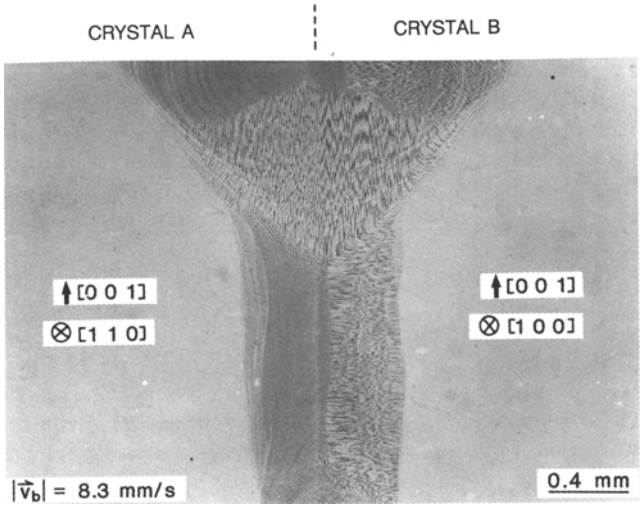

Fig. 17—Transverse-section micrograph of a butt weld made in the $[110]_A/[100]_B$ direction on a (001) surface at 8.3 mm/s.

is intermediate to that found for the 4.2 and 42 mm/ welds (Figures 6 and 7, or 9 and 10). Furthermore, th outer shape is symmetrical with respect to the wel centerline, which supports the earlier conclusion that th weld direction has no influence on the weld pool shape Two samples were welded in this same configuration and they produced the identical composite weld micro structures. As can be seen from Figure 17, the micro structural features of single-crystal weldments made alon [110] (Figure 7) and [100] (Figure 10) directions in single crystal specimens are reproduced with remarkable ac curacy within each half of the bicrystal butt weld. Fo the left half of the weld (welding direction $[110]_A$), th growth of $[100]_A$ dendrites is the preferred growth at th top left and the bottom half of the weld. For the righ half of the weld (weld direction $[100]_B$), the predominan dendrite orientation is $[010]_B$ in the upper and botton parts of the weld. It can be concluded that in these re gions, $\theta > 45$ deg and $\phi > 135$ deg on the left (crystal A) while $\phi < 45$ deg in the right half (crystal B) of the wel pool. In the center of the weld, $[001]_{A,B}$ dendrites grov in both halves of the bicrystal weld, implying that $\theta >$ 45 deg and that ϕ is approximately in the range of 45 t 135 deg. As was the case for welds on the single crys tals, the specific regions of the weld in which a particula dendrite growth occurs are dictated by the pool shape.

Figures 18(a) and (b) show high-magnificatio photomicrographs of the top and bottom halves of transverse section of the butt weld. A careful examina tion of the dendrite orientations in the weld also revealed

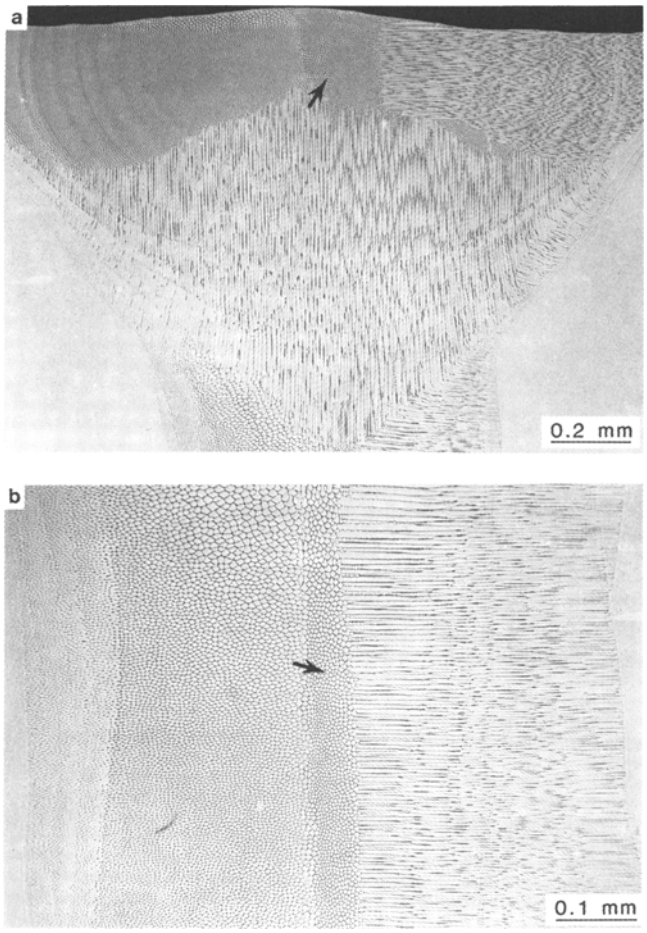

Fig. 18 — Enlargements of the weld shown in Fig. 17 showing details of the microstructure near the (*a*) top and (*b*) bottom of the weld. Arrows point to areas of $[100]_B$ dendritic growth.

the growth of $[100]_B$ dendrites along the welding direction within crystal B. These $[100]_B$ dendrites grow near the top (Figure 18(a)) and along a slender region in the bottom (Figure 18(b)) and are indicated with arrows. They can be distinguished from the $[100]_A$ dendrites growing in crystal A by the fact that they have a smaller and more circular cross section. The $[100]_A$ dendrites grow at a 45 deg angle with respect to the welding direction (and plane of view) and, therefore, appear to be more elliptical in the transverse-section micrograph. The appearance of a small region of $[100]_B$ dendrites near the top is consistent with the single-crystal observations. These dendrites become less stable with increasing welding speed in welds made along the [100] direction, and the size of the zone in which they appear in Figure 18(a) is intermediate to that found for 4.2 and 42 mm/s welds (Figures 9 and 10, respectively). The narrow zone of $[100]_B$ dendrites in the bottom half of the weld is somewhat unexpected since [100] dendrites were not found in the bottom of the weld in either the 4.2 or 42 mm/s welds.

Although it is difficult to assess with any precision how well the weld centerline coincided with the interface between the two crystals, it does not seem that growth from one crystal (say crystal B) is dominating that from the other (crystal A) on a noticeable scale. Figure 19,

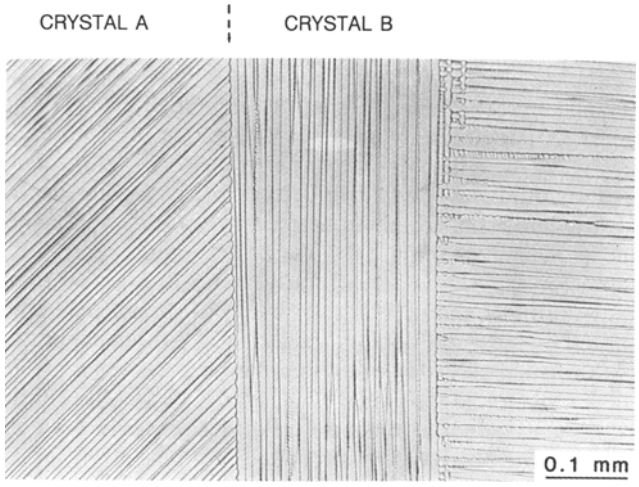

Fig. 19 — Top-section micrograph of the butt weld shown in Fig. 17 showing the growth of dendrites in three directions.

which shows the top surface of this butt weld, clearly indicates that $[100]_B$ dendrites growing parallel to the welding direction do not overtake the $[100]_A$ dendrites, or *vice versa*. A velocity isopleth diagram showing the selected dendrite growth directions as a function of θ and ϕ as well as the velocities of the dendrites is shown in Figure 20 in the form of a stereographic projection. The presence of the three dendrite orientations in the top-view micrograph in Figure 19 is readily understood by referring to this diagram. Along the top surface, ϕ is 0 deg on the right half and 180 deg on the left half of the weld, while θ varies from 90 to 0 deg and back to 90 deg in moving from the right edge to the center and to the left edge of the weld. Figure 20 indicates that $[010]_B$ dendrites should be stable at the right, with $[100]_B$ dendrites

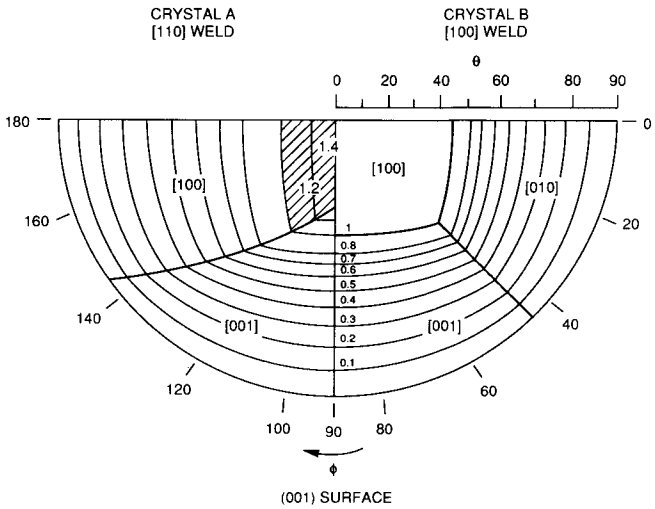

Fig. 20 — Stereographic projection showing the isopleth lines and the transition lines between the various dendrite trunk orientations for the butt weld shown in Figs. 17 through 19 as a function of θ and ϕ. The centerline of the weld, which separates crystals A and B, corresponds approximately to the vertical line (ϕ = 90 deg), whereas the outer trace of the weld (θ = 90 deg) lies on the outer circle. Scales for reading θ and ϕ values are shown on the drawing.

in the middle, and finally, $[100]_A$ dendrites on the left side.

The region that is cross-hatched in Figure 20 is of particular interest. When comparing the velocities of $[100]_A$ and $[100]_B$ dendrite trunk orientations near the center of the weld (Figure 20), one expects that the $[100]_A$ dendrites would grow with a velocity $\approx\sqrt{2}\,|\vec{v}_b|$, whereas the $[100]_B$ dendrites are characterized by $|\vec{v}_{100}| = |\vec{v}_b|$. Since the slower growing $[100]_B$ dendrites require a smaller undercooling, they project further into the liquid, and they normally should outgrow the $[100]_A$ dendrites in the region of the weld pool characterized by the hatched region in Figure 20. By extending the weld centerline from the bottom to the top (Figure 17), it appears that the $[100]_B$ dendrites do indeed extend across the centerline. However, as the precise position of the original interface between crystals A and B with respect to the weld centerline is not known, it is difficult to assess how far the $[100]_B$ dendrites grew across the weld centerline into crystal A. This evaluation is further complicated by the fact that the variation of θ and ϕ with distance from the centerline is also not known. Thus, the prediction that the slower growing dendrites from one crystal should overtake the faster growing dendrites in the other crystal near the centerline cannot be evaluated in detail. Additional experiments are underway to examine this possible effect in more detail.

IV. CONCLUSIONS

Based on the microstructural observations of single crystals welded under a range of conditions and in a variety of configurations, the following conclusions can be drawn:

1. Single-crystal weld microstructures provide valuable information on the 3-D nature of the weld pool since the presence of the different dendritic growth orientations can be related directly to the solidification front orientation.
2. The weld pool shape is not influenced by the crystallographic orientation so that weld pool shapes determined from single-crystal welds apply to polycrystals as well.
3. With increasing welding speed, the weld pool becomes more slender, with a less distinct crown at the top of the weld. In addition, the pool becomes more elongated in the welding direction.
4. The dendritic structures found for single crystals can be applied directly to the case of bicrystal welds and multipass autogenous welds. The same dendritic patterns found in single-crystal welds are reproduced with remarkable accuracy in these latter cases.
5. The dendritic structures that correspond to weld pool shapes predicted by modeling can be directly compared with experimentally observed dendritic patterns, and thus, the models that can predict weld pool shape can be evaluated for their accuracy.

ACKNOWLEDGMENTS

The authors would like to acknowledge the assistance of R.W. Reed, G.C. Marsh, and H.E. Harmon of Oak Ridge National Laboratory in the preparation of the specimens. They would also like to thank Drs. E.A. Kenik and T. Zacharia of Oak Ridge National Laboratory for reviewing the manuscript. This research was sponsored by the Division of Materials Sciences, United States Department of Energy, under Contract No. DE-AC05-84OR21400 with Martin Marietta Energy Systems, Inc.

REFERENCES

1. W.F. Savage, C.D. Lundin, and A.H. Aronson: *Weld. J.*, 1965, vol. 44, pp. 175s-81s.
2. W.F. Savage and A.H. Aronson: *Weld. J.*, 1966, vol. 45, pp. 85s-89s.
3. W.F. Savage, C.D. Lundin, and T.F. Chase: *Weld. J.*, 1968, vol. 47, pp. 522s-26s.
4. J.M. Samuel: Ph.D. Thesis, Rensselaer Polytechnic Institute, Troy, NY, 1979.
5. M.C. Flemings: *Solidification Processing*, McGraw-Hill, New York, NY, 1974, p. 159.
6. W. Kurz and D.J. Fisher: *Fundamentals of Solidification*, Trans Tech Publications Ltd., Aedermannsdorf, Switzerland, 1984, p. 240.
7. M. Rappaz and E. Blank: *J. Cryst. Growth*, 1986, vol. 74, pp. 67-76.
8. H. Nakagawa, M. Katoh, F. Matsuda, and T. Senda: *Trans. Jpn. Weld. Soc.*, 1971, vol. 2 (1), pp. 1-9.
9. M. Kato, F. Matsuda, and T. Senda: *Trans. Jpn. Weld. Soc.*, 1972, vol. 3 (1), pp. 59-68.
10. M. Rappaz, S.A. David, J.M. Vitek, and L.A. Boatner: *Metall. Trans. A*, 1989, vol. 20A, pp. 1125-38.
11. M. Rappaz, S.A. David, J.M. Vitek, and L.A. Boatner: *Metall. Trans. A*, 1990, vol. 21A, pp. 1767-82.